

S-Wave Attenuation Structure in the Taiwan Area and Its Correlation to Seismicity

Kuang-Jung Chen¹

(Manuscript received 8 September 1997, in final form 16 February 1998)

ABSTRACT

S-wave amplitude data from the Taiwan Telemetered Seismographic Network (TTSN) and the Central Weather Bureau Seismographic Network (CWBSN) are used in a tomographical inversion for a three-dimensional S-wave attenuation structure beneath the Taiwan area. The data consist of three-dimensional, digital seismograms of 137 earthquakes with magnitudes between 3.0 and 5.0. The S-wave attenuation structure is obtained through the use of the damped least-squares method from attenuation time value (t^*) and travel times. Attenuation time value is calculated by using the spectral decay method under the assumption that t^* is independent of frequency. S-wave spectra are corrected for a ω^2 source spectrum model. The frequencies of instrument response above 25 Hz or below 4 Hz usually have large uncertainty. Therefore, the least-squares line fitting is performed in the frequency band of 4 to 25 Hz. The results here show that the distribution pattern of the Q_s values in the Taiwan area correlates well with seismicity. In the upper crust (depths of between 0 to 15 km), the region of lower Q_s area correlates with higher seismicity. However, in the lower crust and upper mantle (15 to 75 km), the area of higher seismicity correlates with the regions of higher Q_s values.

(Key words: Q_s structure, Attenuation time value, Seismicity)

1. INTRODUCTION

The anelasticity of the Earth, as measured by the specific quality factor Q , has long been recognized as an important indicator of the composition, state and temperature of the deep interior. This seismic parameter is not well understood and is often difficult to measure. However, its measurement is essential for the prediction of ground motion produced by earthquakes or explosions, the determination of earthquake magnitude, the understanding of regional geodynamics and the evaluation of seismic risk. Attenuation estimates are also very useful in characterizing certain physical properties of rock materials that cannot be inferred from seismic velocities.

¹Institute of Earth Sciences, National Taiwan Normal University, Taipei, Taiwan, ROC

Studies on the attenuation of seismic waves have occupied a significant portion of seismic literature over recent years (Der and McElfresh, 1976; Al-Shunkri *et al.*, 1988; Kanamori, 1967a; 1967b; Lee and Solomon, 1978; Solomon, 1972; 1973; Teng, 1968). Attenuation measurements can carry much information regarding the physical state of the Earth's interior and are important in making corrections in source mechanism studies. Observations of lateral variations in Q may aid in determining regional differences in temperature, phase and composition.

The tectonic features of the Taiwan area are extremely complicated because of the nearby convergence of the Eurasian and Philippine Sea plates. The collision of the Philippine Sea and Eurasian plates as well as the spreading of the Okinawa Trough are the main reasons for the complex geological structures and high seismicity in this region (Figure 1). Roecker *et al.* (1987) applied a three-dimensional block inversion method to obtain the velocity structure of this area and reported the existence of velocity heterogeneity in the uppermost mantle. It is believed that the high-velocity zones are generally associated with the subducted Philippine Sea plate. Moreover, Chen (1993) investigated the corresponding attenuative property of P-waves beneath this region. He pointed to the presence of a high- Q_p zone associated with the subducted Philippine Sea plate in northeastern Taiwan and the subducted Eurasian plates in the south.

Chen *et al.* (1996) determined the Q_p structure in the Taiwan area and its correlation with seismicity. In the present study, seismic data as recorded by the TTSN and CWBSN are used to obtain a three-dimensional model of the Q_s structure beneath the Taiwan area. Figure 2 shows the distribution of the stations for these two networks. The CWBSN has 75 stations including (those of) the TTSN stations. These authors expect that the Q_s structure provide useful information for a better understanding of the material beneath this area. For this purpose, the spectral decay of the seismic S phase is used as basic observed data. The three-dimensional Q_s structure is parameterized by 9 layers bounded by horizontal interfaces, each of which is separated into a mesh of rectangular prisms by two orthogonal sets of vertical interfaces (see Figure 6). Totally, the study region is divided into 940 "blocks". The interfaces (including horizontal and vertical) are similar to those of the velocity model IV3 used by Roecker *et al.* (1987). The Q_s values in these blocks are estimated as the output of an inverse problem from the observed data.

2. SPECTRAL DECAY METHOD

Q is a dimensionless quantity that measures the amount of energy dissipated per radian as seismic waves propagate. In other words, a seismic wave loses $1/Q$ of its energy after traveling each radian owing to the anelasticity of the medium. Laboratory studies have previously shown Q to be independent of frequency (Knopoff, 1964). However, theoretically, Q varies significantly with a function of frequency for a rock sample of uniform composition and grain size (Hough and Anderson, 1988). Also, in a composite viscoelastic model with a range of relaxation times, Q varies smoothly with frequency and may be considered (to be) constant over a narrow frequency band (Kanamori and Anderson, 1977). The basic assumption that Q is independent of frequency within the interested frequency band is often made in studies of seismic

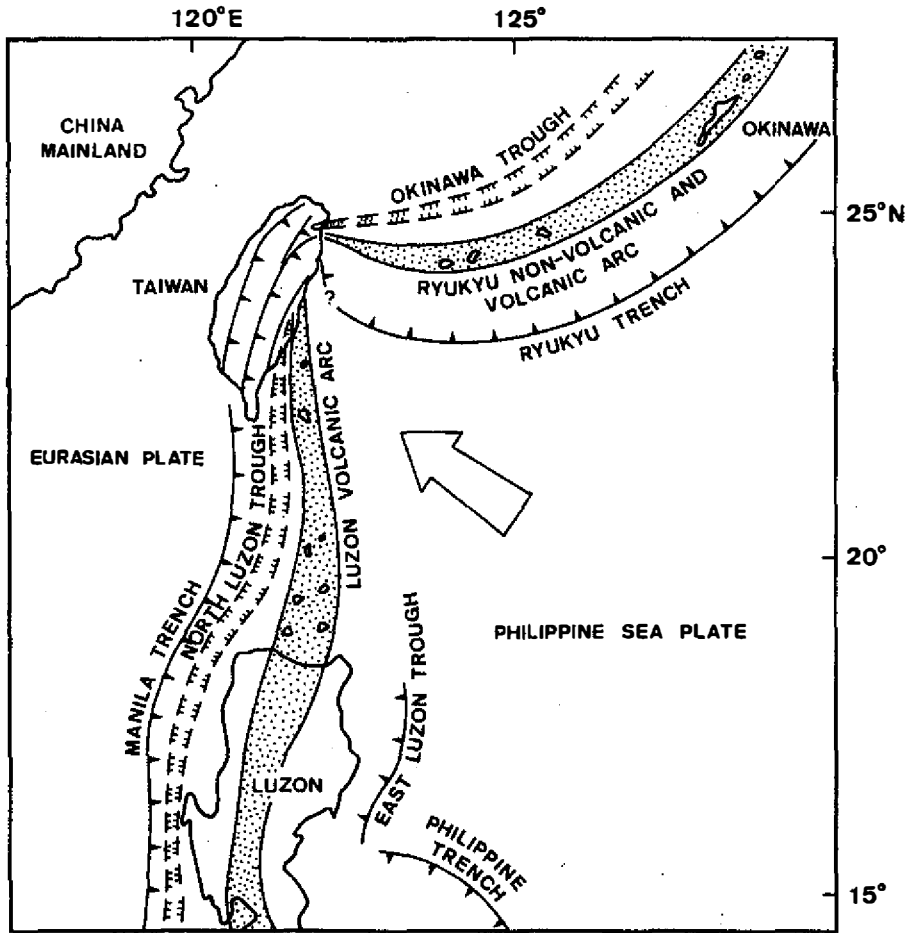


Fig. 1. Regional plate tectonic setting of Taiwan and the neighboring region (after Ho, 1986), showing the interaction of the Philippine Sea and Eurasian plates in Taiwan with the Ryukyu arc system developing to the east and northeast, and the Luzon arc system extending to the south.

wave attenuation using the reduced spectral ratio technique (Teng, 1968; Solomon, 1972; 1973).

The effect of Q on a seismic signal along a ray path describes the variation of the displacement spectrum $A(r, f)$, namely:

$$A(r, f) = A_0(r, f)e^{-\pi f t^*}, \tag{1}$$

where

$$t^* = \int_0^s \frac{dr}{QV} \tag{2}$$

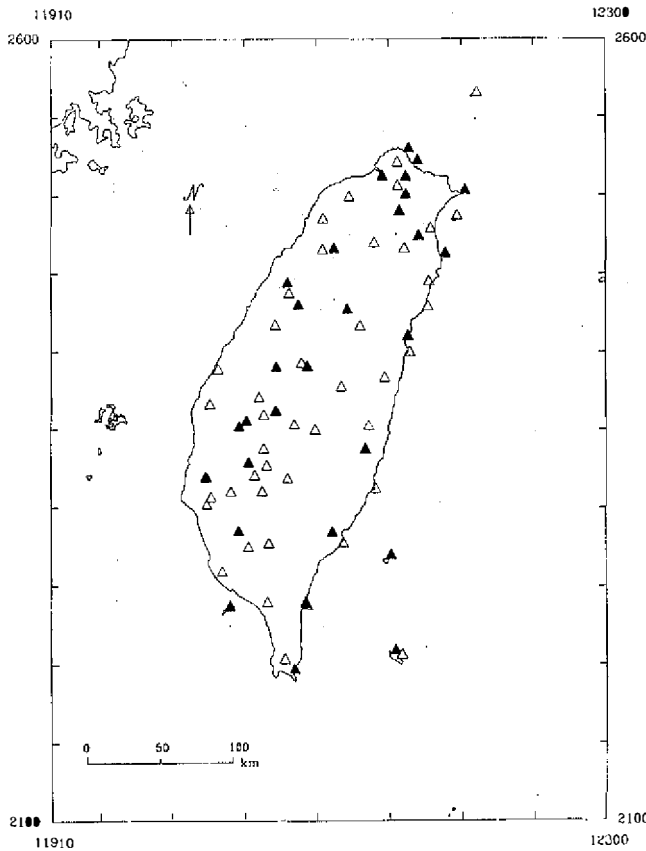


Fig. 2. Geographical locations of the TTSN (solid triangles) and the CWBSN (solid and hollow triangles).

in which V is the wave velocity, Q is the spatial attenuation factor, and the integral is along the ray path s (Kanamori, 1967a). The spectrum of displacement, observed at a site distance r from the epicenter, $A(r, f)$, may be approximated by:

$$A(r, f) = (2\pi f)^2 S(f) I(f) G(r, f) e^{-\pi f t^*} \quad (3)$$

where $G(r, f)$ gives the effect of geometrical spreading that is usually assumed to be independent of frequency, $I(f)$ is the instrumental response, and $S(f)$ is the displacement spectrum of radiation at the source. In a homogeneous medium, $G(r, f)$ can be approximated by $1/r$ for body waves. At high frequencies, a widely accepted source spectrum model is the ω^2 model, which assumes that $S(f)$ is proportional to f^{-2} (Brune, 1970; Hanks, 1979). This model was used to study the attenuation of high-frequency waves from teleseismic sources (Der and McElfresh, 1976; 1977; Lundquist and Cormier, 1980; Der *et al.*, 1982; 1985), and at regional distance (local earthquakes) (Modiano and Hatzfeld, 1982; Hough and Anderson, 1988; Hough *et al.*, 1988). Since the primary interest here is not the absolute value of t^* but rather its spatial variation within the crust, assuming a ω^2 model should present no difficulties in drawing conclusions. Under this assumption, $A_0(r, f)$ in Equation (1) becomes independent of frequency.

Since the instrumental response $I(f)$ is usually known for each component at all stations, the effect can be removed from the above spectrum $A(r, f)$. In other words, Equation (1) can be rewritten, after taking the natural logarithm on both sides, as:

$$\ln A(r, f) = \ln A_0(r) - \pi f t^* . \quad (4)$$

The term $A_0(r)$ in Equation (4) includes the geometric spreading effect, which is independent of frequency. Since the spreading effect is frequency-independent, the value of $A_0(r)$ only affects the level of the spectrum but has no effect on the observed t^* . If Q is frequency-independent, then t^* is also frequency-independent. Thus, Equation (4) shows $\ln A(r, f)$ as a straight line in f and can be differentiated with respect to f to obtain the t^* :

$$\frac{d(\ln A(r, f))}{df} = -\pi t^* . \quad (5)$$

The corrected observations, in $A(r, f)$, is fitted to a straight line by using the least-squares method over a frequency range extending somewhat beyond the corner frequencies. However, many studies have pointed out that Q is frequency-dependent in the crust under the continental regions, at least at frequencies near 1 Hz (for example: Mitchell, 1980), and the degree of the dependence varies regionally (Mitchell, 1981). But unfortunately, it is almost impossible to investigate the frequency-dependency of Q with the data available in this study. Since the primary goal here is to find the spatial variations of attenuation in the upper crust of the Taiwan area, the use of frequency-independent attenuation is assumed. For earthquakes used in this study, the corner frequencies range from about 1 to 4 Hz. A frequency band of 4-25 Hz is chosen in this study. The former is limited by the corner of the source frequency, while and the latter is limited by the uncertainty in instrument response above 40 Hz.

3. DATA AND COMPUTATION

Digital seismograms from 137 (from 1987 to 1994) local events in the Taiwan region are used to obtain the body-wave spectra. A total of 1523 t^* values are obtained. The magnitudes of these earthquakes range from 3.0 to 5.0. Figure 3 shows the location of these earthquakes and the seismic stations used in this study. The first 2.0 second starting from the onset time of the S-waves of the seismograms are analyzed in term of S phase. The Fast Fourier Transform (FFT) method is used to study the S phase spectra. A frequency band from 4 to 25 Hz is selected in this study. The spectrum for frequencies lower than the corner-frequency and eigen-frequency are rather unreliable, while that for those higher than 25 Hz has a very small amplitude due to a high cut-off filter in the recording system. The slope for the Fourier spectrum versus frequencies is determined by using the method of least squares. The procedure for determining the spectrum and calculating the attenuation of body waves is basically the same as that used by Hough *et al.* (1988) and Al-Shukri *et al.* (1988). The only difference between the present study and that of Hough *et al.* (1988) is that a Parzen window is used here, whereas a cosine window before spectral analysis was used in the earlier study. It is found that the Parzen window produces a smoother spectrum than the cosine window does. Consequently, it

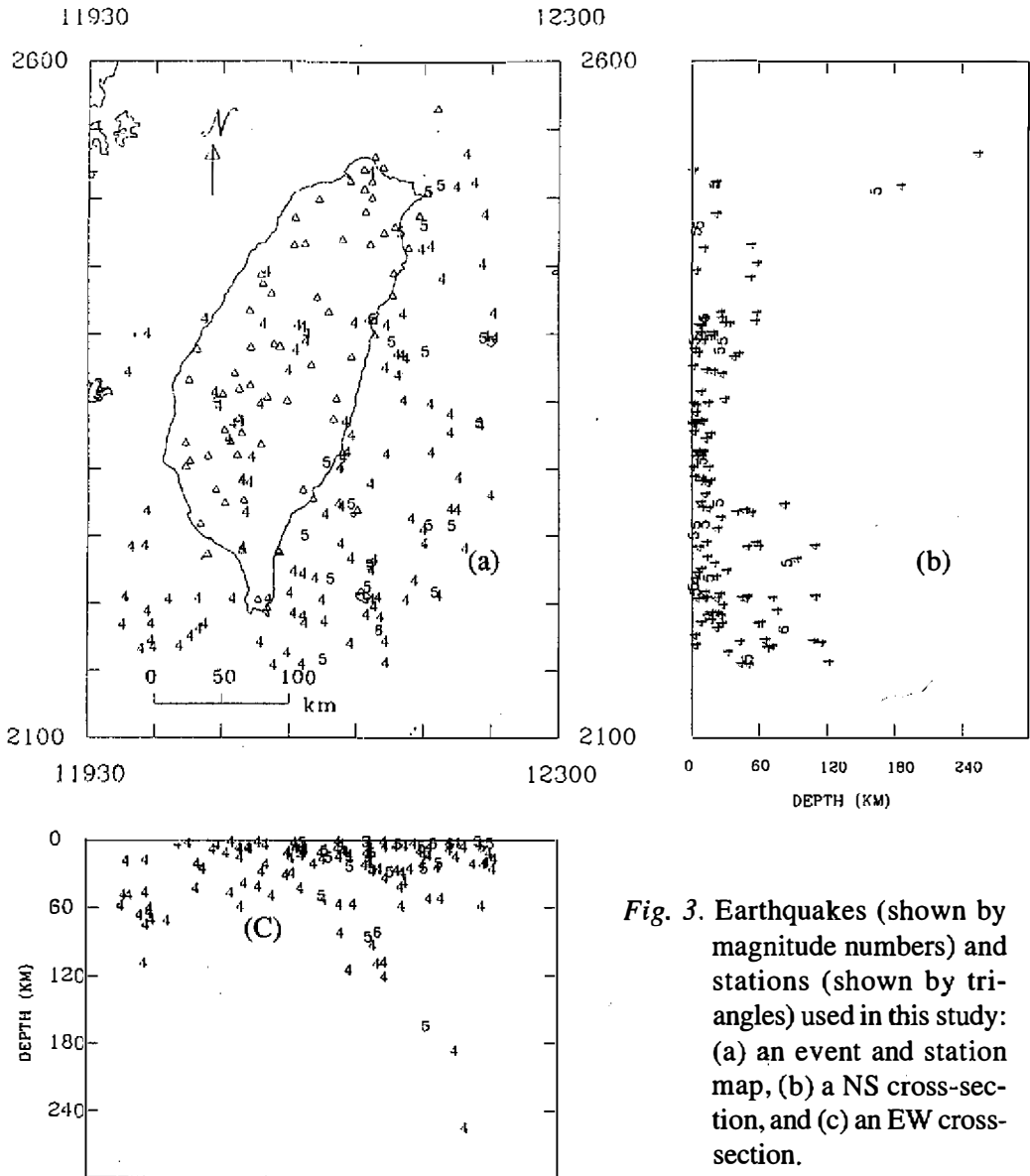


Fig. 3. Earthquakes (shown by magnitude numbers) and stations (shown by triangles) used in this study: (a) an event and station map, (b) a NS cross-section, and (c) an EW cross-section.

enables the elimination of the need for smoothing the spectrum before fitting the general trend with the least-squares method. The smoothing of the power spectrum also eliminates the effect of variance in the instrument response. Figure 4a shows a sample of one seismogram used for calculating the t^* value and S wave window. The truncated data by the time window is shown in Figure 4b. Figure 4c shows the spectra calculated from the data in Figure 4b. The regression line and the t^* value are shown in Figure 4c. The error of t^* (± 0.0051 shown in Figure 4c) is contributed by the deviation between each of the observed values and the corresponding calculated values from the line regression.

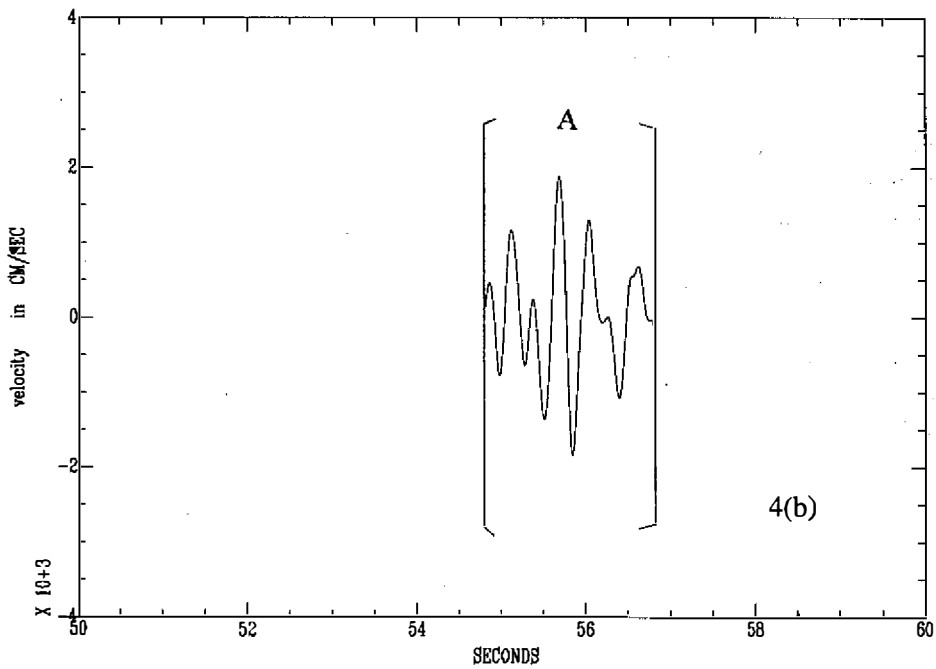
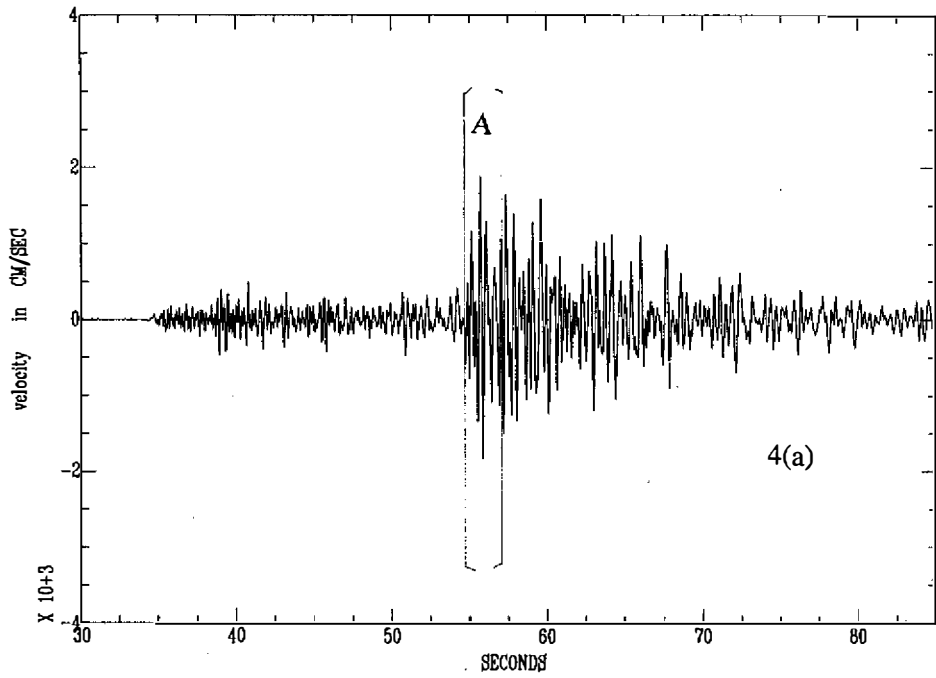
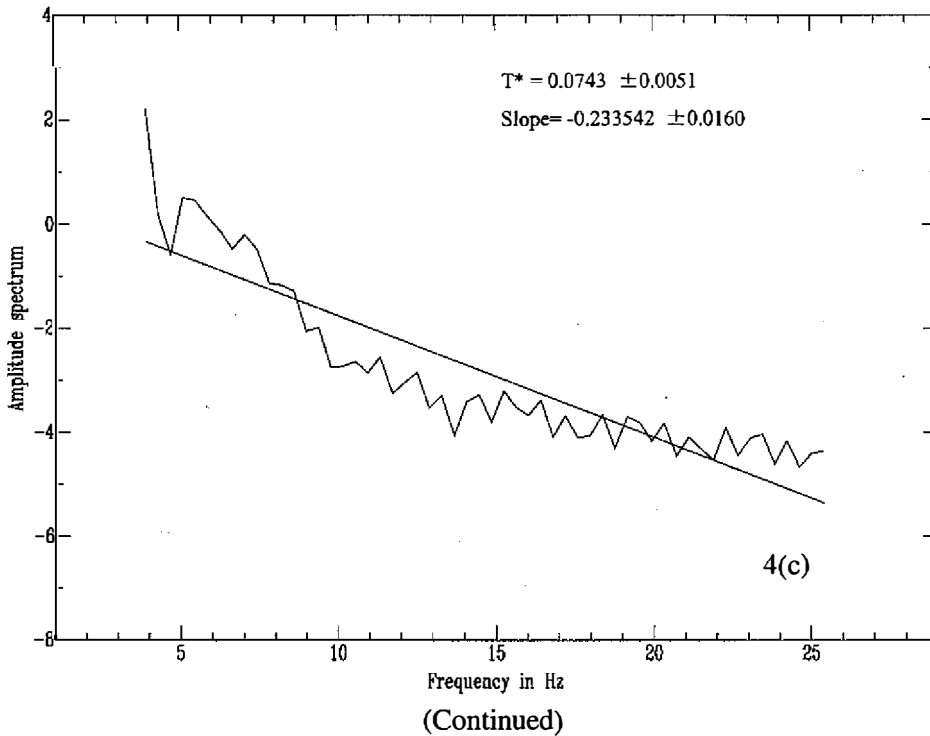


Fig. 4. (a) Seismogram used for calculating the t^* value and the time window A (b) the truncated data by time window A (c) spectra calculated from the truncated data in (b); the regression line and the t^* value are also shown.



4. LINEARIZED INVERSION FOR S-WAVE ATTENUATION

A least-squares inversion scheme is developed here to determine a three-dimensional image of attenuation within a specific volume of the Earth beneath a local or regional seismic network. Data used for this technique are the observed t^* values calculated from S-waves. The inversion procedure starts by separating the volume of the crust and upper mantle beneath Taiwan into a number of layers, each layer being subdivided into a number of rectangular blocks; in each block both the velocity and attenuation are assumed to be constant. The attenuation within each block is denoted as Q_j^{-1} , where j is an index of a certain block. The discretization permits the calculation of the initial t^* for each ray that traverses the starting model. For a crustal model with discrete values of velocity and Q_j^{-1} in each block, Equation (2) becomes:

$$t^* = \sum_{j=1}^M t_j Q_j^{-1} \delta_j \quad , \quad (6)$$

where M is the number of blocks in the model; δ_j is a delta function equal to unity inside each block that has been traversed by a ray and zero otherwise; Q_j^{-1} is a value for attenuation; and t_j is a value for the travel time in each block of the initial model. Assuming that the observed t_{ob}^* can be parameterized in a function similar to that in Equation (6), the difference between

t_{ob}^* and t^* can be written as:

$$\delta t^* = \sum_{j=1}^M \delta_j t_j \left(\frac{t_{ob}}{t_j} Q_{ob}^{-1} - Q_j^{-1} \right), \tag{7}$$

where Q_j^{-1} is the unknown value of attenuation in each block. For N observations, a set of equations can then be formed as :

$$\begin{bmatrix} \delta t_1^* \\ \cdot \\ \cdot \\ \cdot \\ \delta t_N^* \end{bmatrix} = \begin{bmatrix} t_{11} & t_{12} & \cdot & \cdot & t_{1M} \\ t_{21} & \cdot & \cdot & \cdot & \cdot \\ \cdot & \cdot & \cdot & \cdot & \cdot \\ \cdot & \cdot & \cdot & \cdot & \cdot \\ t_{N1} & \cdot & \cdot & \cdot & t_{NM} \end{bmatrix} \begin{bmatrix} \delta Q_1^{-1} \\ \delta Q_2^{-1} \\ \cdot \\ \cdot \\ \delta Q_M^{-1} \end{bmatrix}, \tag{8}$$

where δQ_j^{-1} is the unknown attenuation perturbation ($Q_{ob}^{-1} - Q_j^{-1}$) for the j th block through which rays have traveled for a particular period of time. Note that t_{ij} in Equation (8) is the theoretical travel time in the j th block from the i th observation. Equation (8) can be rewritten in matrix form as:

$$\mathbf{Y} = \mathbf{T} \mathbf{q}, \tag{9}$$

where \mathbf{Y} is the δt^* vector, \mathbf{T} is the travel-time matrix, and \mathbf{q} is the unknown vector of attenuation. A stochastic least-squares solution to Equation (8) is given by

$$\hat{\mathbf{q}} = \left[\mathbf{T}^T \mathbf{T} + \theta^2 \mathbf{I} \right]^{-1} \mathbf{T}^T \mathbf{Y}, \tag{10}$$

where $\hat{\mathbf{q}}$ is the approximate solution of \mathbf{q} , θ^2 is the damping parameter with a positive value, and \mathbf{I} is the identity matrix. Equation (9) is an overdetermined system due to the expected errors in the observations and t_{ob}^* using the spectral decay technique. The stochastic least-squares solution is preferred because it is more stable than the undamped solution. The resolution matrix for the solution is given by:

$$\mathbf{R} = \left[\mathbf{T}^T \mathbf{T} + \theta^2 \mathbf{I} \right]^{-1} \mathbf{T}^T \mathbf{T}, \tag{11}$$

and the covariance matrix by:

$$\mathbf{C} = \sigma_d^2 [\mathbf{T}^T \mathbf{T} + \theta^2 \mathbf{I}]^{-1} \mathbf{T}^T \mathbf{R}, \quad (12)$$

where σ_d^2 is the variance of error in the data. The standard errors of the solution are equal to the square roots of the diagonal elements of \mathbf{C} . Here, the initial θ^2 is set to 10. Whenever an inverted Q_s are negative, adding a larger θ^2 to the corresponding Q block is needed until that inverted Q_s become positive. But the larger the θ^2 is set, the more overestimated are the Q_s values. The average of θ^2 in this study is approximately 1000. The above scheme allows for the final solution to be obtained interactively and for the examination of the convergence of the solution at each step.

The essential step of the forward solution for setting up Equation (8) is the calculation of the travel-time matrix. The travel-time traced by a ray in each individual block is calculated by using a ray-tracing algorithm in which blocks are assumed to be homogeneous and rays within these blocks are characterized by approximately straight-line paths. Thurber and Ellsworth (1980), using numerical integration through a heterogeneous medium, obtained an excellent approximation to the actual travel time. In the present study, a numerical integration procedure similar to the one used by Thurber and Ellsworth (1980) is employed to calculate the travel time. First, the ray is classified into a number of segments having equal lengths. Then, the travel time for each segment is calculated, and the times of all segments belonging to the same block are added together to form the total travel time in that block. If a ray hits a block or a layer boundary, the length of the segment is modified such that it is the distance between the end of the last segment and the boundary. The travel time for this modified segment is calculated accordingly. In this study, the S-wave velocity model inverted by Roecker *et al.* (1987) is used to calculate the travel times. The earthquakes used in this study are relocated using the velocity model mentioned above. The event with an error of relocation (ERH and ERZ) beyond 5 Km is discarded.

The inversion procedure is tested extensively. Both homogeneous and heterogeneous models are first used to generate synthetic data for t^* . In order to be certain that the inversion program is correct, some different percentages of error are added to t^* and the inversion is performed to obtain Q values. The velocity and Q model for testing is shown Figure 5a. The numbers denote the block number. Its corresponding velocity and Q values are shown within the parentheses. The "true" travel times and "true" t^* can be calculated from this model. Subsequently, some variances are added to the "true" t^* and "true" travel times to examine the amounts that attribute to the inverted Q values. Figure 5b shows the results. It is found that the difference between the inverted and the "true" Q is proportional to the percentage of input errors. The results indicate that the inversion program here is proper. These data are then inverted by using a number of different starting models. In the foregoing calculations, the initial value of Q_s is set at 0. Then the average Q_s values are estimated and used to check the dependence of the results for initial values. An average Q_s of 0.0005 is obtained. The results indicate that the initial values do not influence the evaluated Q_s values to any great extent. In all cases, with a sufficient number of observations, solutions using error-free synthetic data

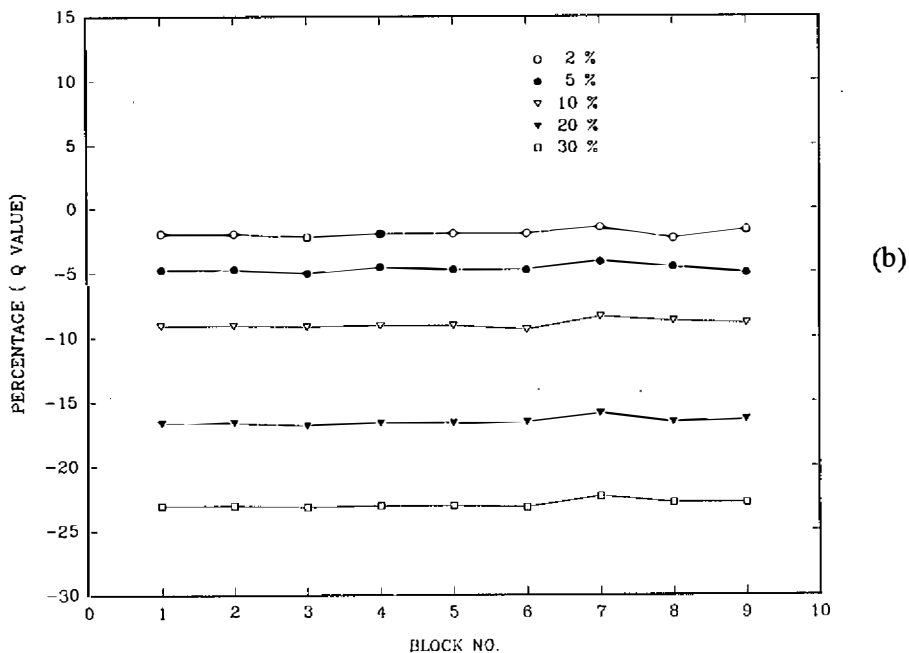
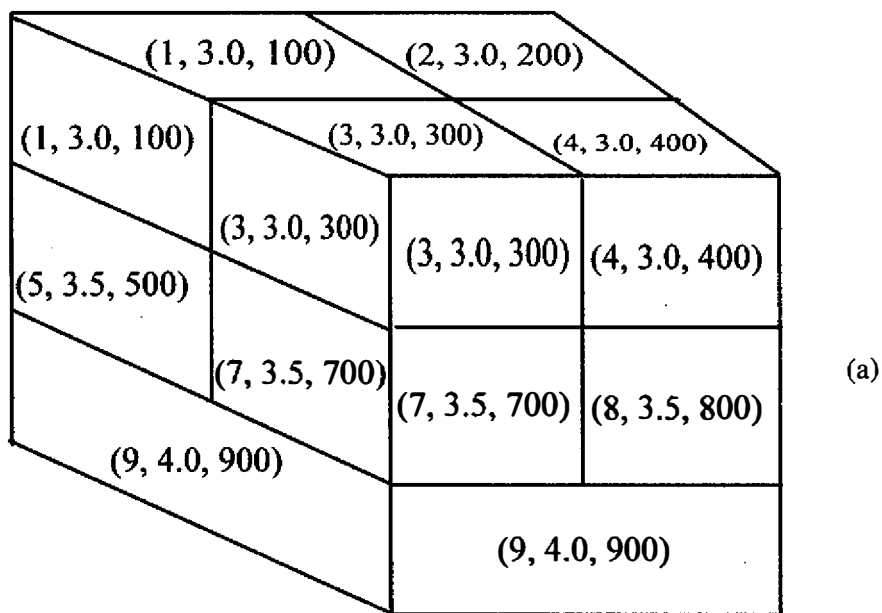


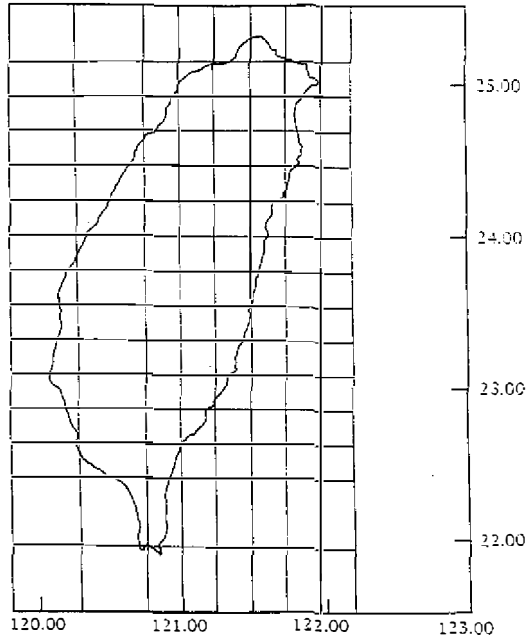
Fig. 5. (a) "True" velocity and the Q model used to test the inversion program; the numbers shown within the parentheses denote block number, velocity, and Q value (b) Percentages of deviation between the inverted and true Q values, corresponding to the different input errors.

LAYER 2

						207.0	
				88.0	268.8	0.93	277.0
				0.93	0.93	5.2	0.93
				5.2	4.1		4.0
				255.0	438.0	185.0	182.2
				0.93	0.93	0.93	0.93
				4.6	4.9	5.1	4.8
				130.9		151.3	130.0
				0.93		0.92	0.92
				3.8		2.3	2.7
				50.0	196.2	315.5	105.0
				0.93	0.93	0.93	0.93
				3.5	2.3	1.4	3.3
				392.2	287.4	389.1	288.0
				0.93	0.93	0.93	0.93
				1.8	1.6	1.8	1.9
				164.2	135.0	181.0	
				0.93	0.93	0.94	
				1.5	6.0	6.4	218.0
							6.3
				204.0		805.0	392.9
				0.94		0.93	0.93
				8.2		5.7	5.5
				88.0		315.5	140.0
				0.93		0.93	0.93
				5.4		3.7	4.5
				106.0	215.1	188.0	458.0
				0.93	0.93	0.93	0.93
				4.9	3.4	4.3	4.8
				140.0	355.0	303.0	
				0.93	0.93	0.93	
				5.1	5.2	5.2	
				158.0		714.3	90.0
				0.93		0.72	0.73
				5.2		4.4	4.5
				266.0	300.0	59.0	151.0
				0.83	0.88	0.89	0.89
				4.9	5.0	5.1	5.1
						44.0	235.0
						0.91	0.91
						5.1	5.1
				60.0			
				0.91			
				5.1			
				5.0		10.0	KM

Layer 2 (5~10 km)

6(b)

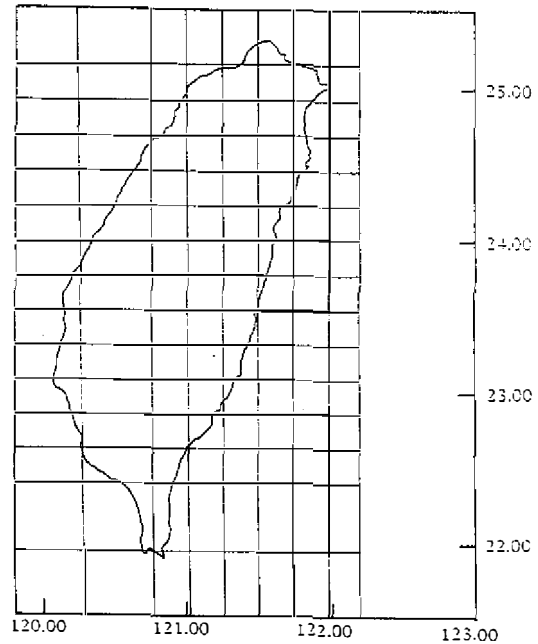


LAYER 3

						396.4	
				224.7	138.0	322.0	538.5
				0.92	0.93	0.93	0.93
				2.9	4.1	4.6	4.5
				173.3	158.7		558.0
				0.93	0.93		0.93
				2.7	2.3		2.5
				495.0	649.3	143.0	176.7
				0.93	0.93	0.93	0.93
				1.5	1.2	3.2	1.9
				225.0	163.9	515.0	139.3
				0.93	0.93	0.93	0.91
				3.7	2.2	3.7	184.2
				122.7	217.0	413.5	109.0
				0.93	0.93	0.93	0.93
				1.3	1.2	1.3	1.3
				339.0	338.0		
				0.93	0.93		
				3.2	3.3		
				65.0	290.7	320.0	265.0
				0.83	0.93	0.93	0.93
				4.3	2.4	3.8	4.5
						266.0	
						0.93	279.0
						4.8	4.8
				426.0		138.0	183.0
				0.93		0.93	0.93
				4.8		5.0	5.0
				188.0	150.0	195.7	152.0
				0.93	0.93	0.93	0.93
				5.1	5.2	3.3	3.6
				233.0		205.0	
				0.93		0.93	
				4.2		4.2	
					135.0	208.0	185.0
					0.93	0.93	0.93
					4.7	5.0	5.0
				286.0	101.0		348.0
				0.93	0.93		0.93
				5.1	5.1		5.1
						233.0	
						0.93	
						5.1	
				10.0		15.0	KM

Layer 3 (10~15 km)

6(c)



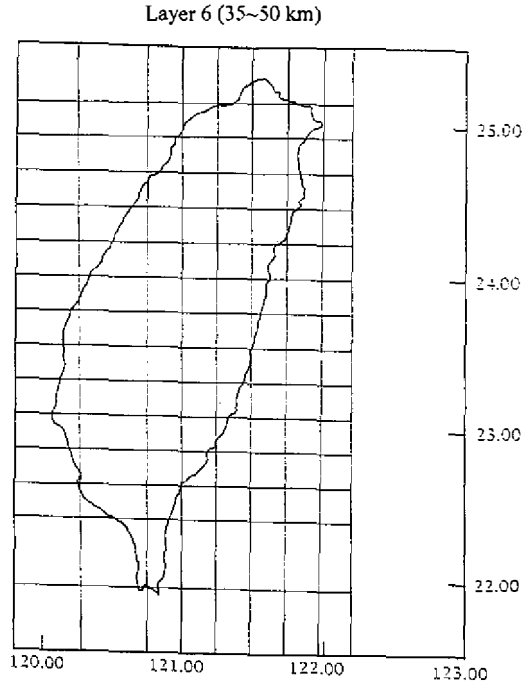
(Continued)

LAYER 6

					140.6 0.93 3.5	174.0 0.93 3.5			
					1136.4 0.95 2.6	1087.0 0.95 2.6			
					1030.9 0.94 2.1	1315.8 0.94 2.2	2631.6 0.94 2.2		
		342.5 0.91 1.3	1639.3 0.91 1.4		352.1 0.92 1.8	906.0 0.93 3.5	780.0 0.93 3.7		
		281.7 0.93 2.0	1020.4 0.93 1.8	954.0 0.93 3.5	1123.6 0.96 2.9	505.0 0.94 2.5	733.0 0.94 2.5		
					701.0 0.94 2.6				
			520.8 0.94 2.4			704.0 0.94 3.8	808.0 0.93 4.0		
		502.0 0.93 4.3		653.0 0.93 4.3					
		800.0 0.93 3.3		813.0 0.93 2.1	1030.9 0.93 1.4	343.6 0.91 0.9	892.0 0.91 2.0		
	703.0 0.92 3.6	886.0 0.93 2.6	2080.0 0.93 2.2		347.2 0.93 2.1				
	606.0 0.93 2.9		340.1 0.66 2.1	321.0 0.79 3.7	445.0 0.60 3.7				
				296.0 0.90 3.7					
		593.0 0.92 4.4	399.0 0.88 4.6		724.6 0.89 4.0		805.0 0.90 4.1		
		229.0 0.81 4.7	388.0 0.92 4.8		237.5 0.92 4.6				
	380.0 0.92 4.9	390.0 0.92 4.9							

35.0 - 50.0 KM

6(f)

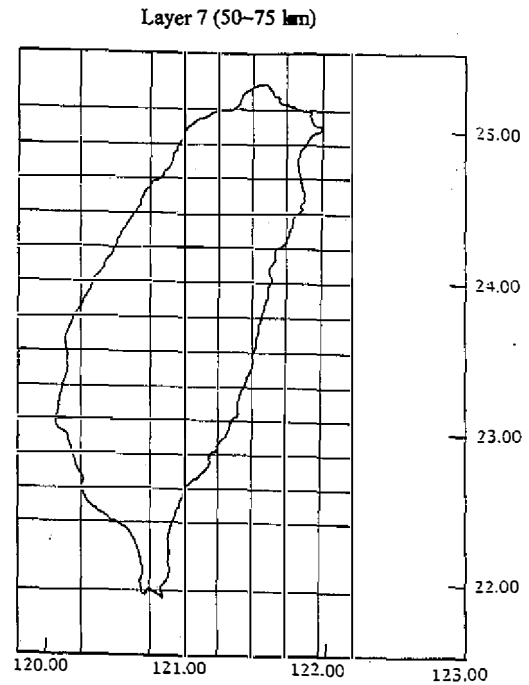


LAYER 7

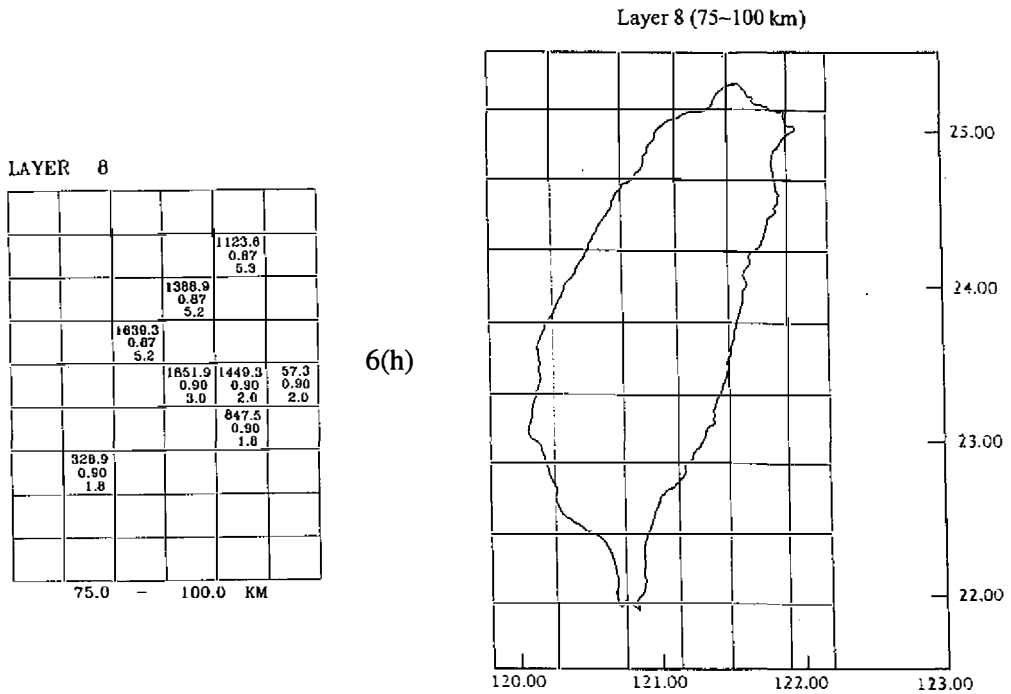
								1205.0 0.92 4.9	
				507.6 0.93 3.8	528.1 0.93 3.1	446.4 0.98 2.9	2222.2 0.96 2.9		
				301.2 0.94 2.4	454.5 0.94 2.5	438.7 0.94 2.5			
					1075.3 0.96 2.6	653.8 0.95 2.7	362.3 0.95 2.7		
		414.0 0.94 3.9	955.0 0.93 4.6	2040.8 0.93 4.1			502.5 0.93 4.0		
			1063.0 0.93 4.0						
			3030.3 0.95 2.6	2088.0 0.95 2.9			135.3 0.95 2.8		
			2053.0 0.94 3.4		1618.2 0.94 2.3	1204.8 0.93 1.8	446.4 0.93 1.7		
		1886.8 0.50 2.0	998.0 0.71 3.6	1298.7 0.72 3.5					
	181.2 0.73 3.4				578.0 0.75 3.3				
	380.2 0.75 3.3								
		757.6 0.62 4.3	478.5 0.70 3.7		680.0 0.71 3.8				
		925.9 0.77 4.7	653.6 0.81 4.3		633.0 0.81 4.3				
			617.3 0.87 5.3	220.7 0.87 5.3					
					153.0 0.87 5.3				

50.0 - 75.0 KM

6(g)



(Continued)



(Continued)

In fact, however, Figure 6a shows no such trend. Moreover, the model shows no difference in attenuation between the northern part and the southwestern part of Taiwan where the alluvium is about 1 km thick. This indicates that the alluvial cover has only a very small effect on the Q_s values in the blocks. Earthquakes with magnitude greater than 4.0 located in this layer are plotted in Figure 7a. About 85% of the events occurred in zone ≤ 200 of the Q_s values (Figure 7a). In high Q_s zones (greater than 600), only 5% of the earthquakes occurred.

In layer 2 (depths of between 5 and 10 km), the Q_s values range between 44 and 805 (Figure 6b). About 50% of the Q_s values are less than 180. The average for this layer is 150. The lowest value occurs in a region of intense earthquake activity, while the highest values occur in the outer blocks far away from the active region. Four local Q_s highs are in alignment with the north-south direction parallel to the Coastal Range. More than 96% of events located in this layer are in Q_s zones lower than ≤ 400 (Figure 7b).

In the depth range of 10 to 15 km (layer 3), the Q_s values range from 88 to 649 (Figure 6c) with an average of 230. About 55% of the Q_s values are less than 200. The standard error of each block is slightly less than 5. About 60% of the earthquakes are located in zone ≤ 400 of Q_s . While 30% of the events occur located in Q_s zones lower than 200 (Figure 7c).

In the depth range of 15 to 25 km (layer 4), the Q_s values are distributed from 58 to 1200 (Figure 6d). With approximately 25% of the blocks having Q_s values of less than 200. About 55% of the blocks have Q_s values between 400 and 500. The average of this layer is 300. The average standard error for this layer is 4. Two significant Q_s highs align parallel to the Central

Layer 1 (0 - 5 km)

Layer 2 (5 - 10 km)

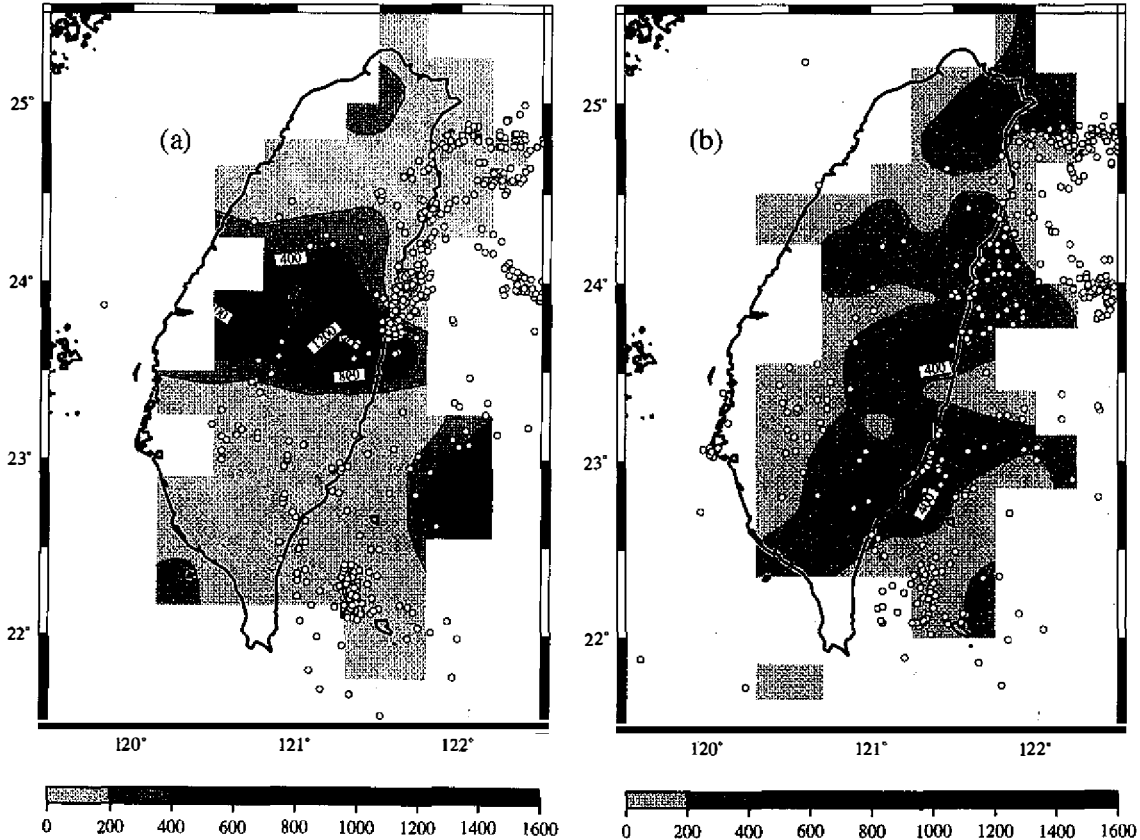


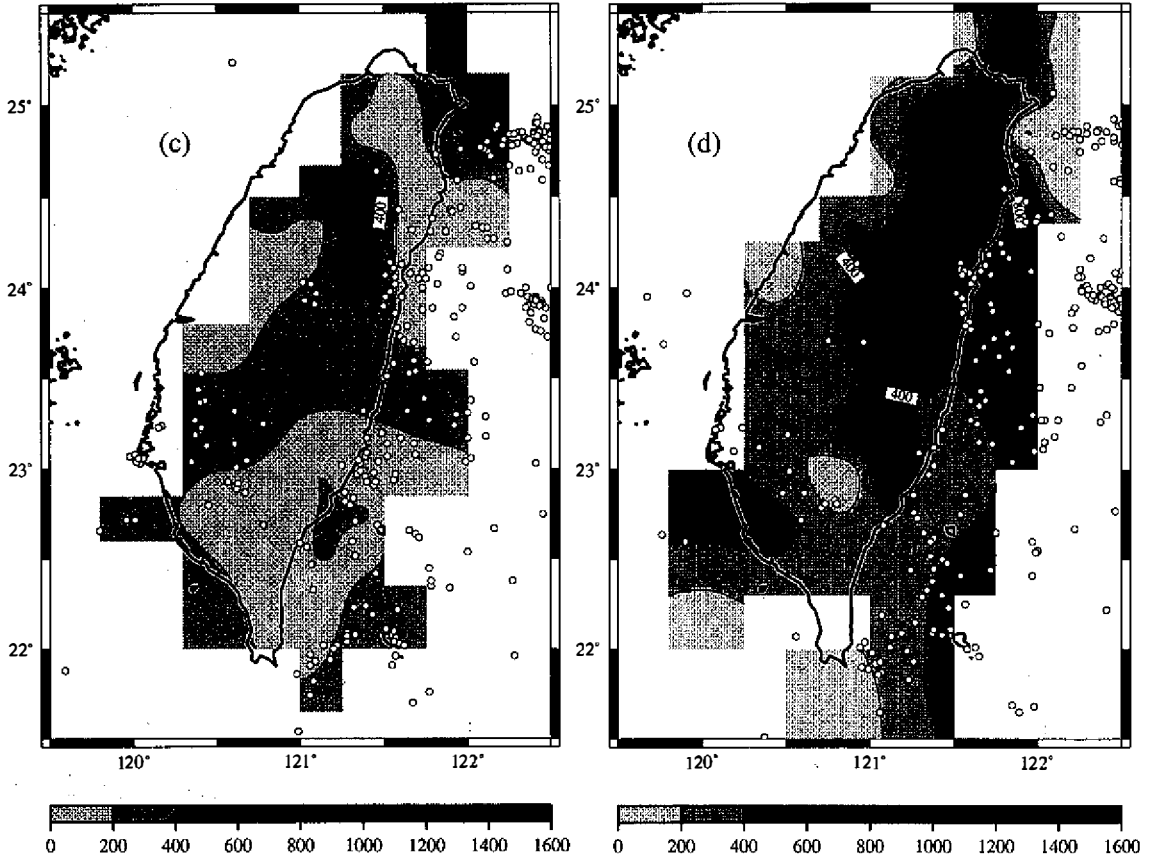
Fig. 7. (a)-(h) Distribution of the Q_s values for each layer. These values are attributed to the center of each block, so that contour lines can be drawn. Contour lines are not drawn on zones through which no ray passes. Earthquakes located in the same block are indicated by hollow circle symbols

Range. There is a Q_s low off the Ilan Plain. The other side of the Ilan Plain is Q_s high. Almost 50% of earthquakes occurred in 600 of Q_s zones (Figure 7d).

In the depth range of 25 to 35 km (layer 5), the Q_s values range between 55 and 925 (Figure 6e) and reveal an average of about 400. About 50% of the blocks have Q_s values less than 400. The standard error is slightly less than 6. The Q_s values increase gradually from northwest to southeast. Three significant highs parallel to the eastern coast of Taiwan. The local Q_s low off the Ilan Plain still exist. More than 93% of earthquakes occurred in Q_s zones lower than 600. About 80% of earthquakes were located in Q_s zone between 400 and 600 (Figure 7e).

Layer 3 (10 - 15 km)

Layer 4 (15 - 25 km)



(Continued)

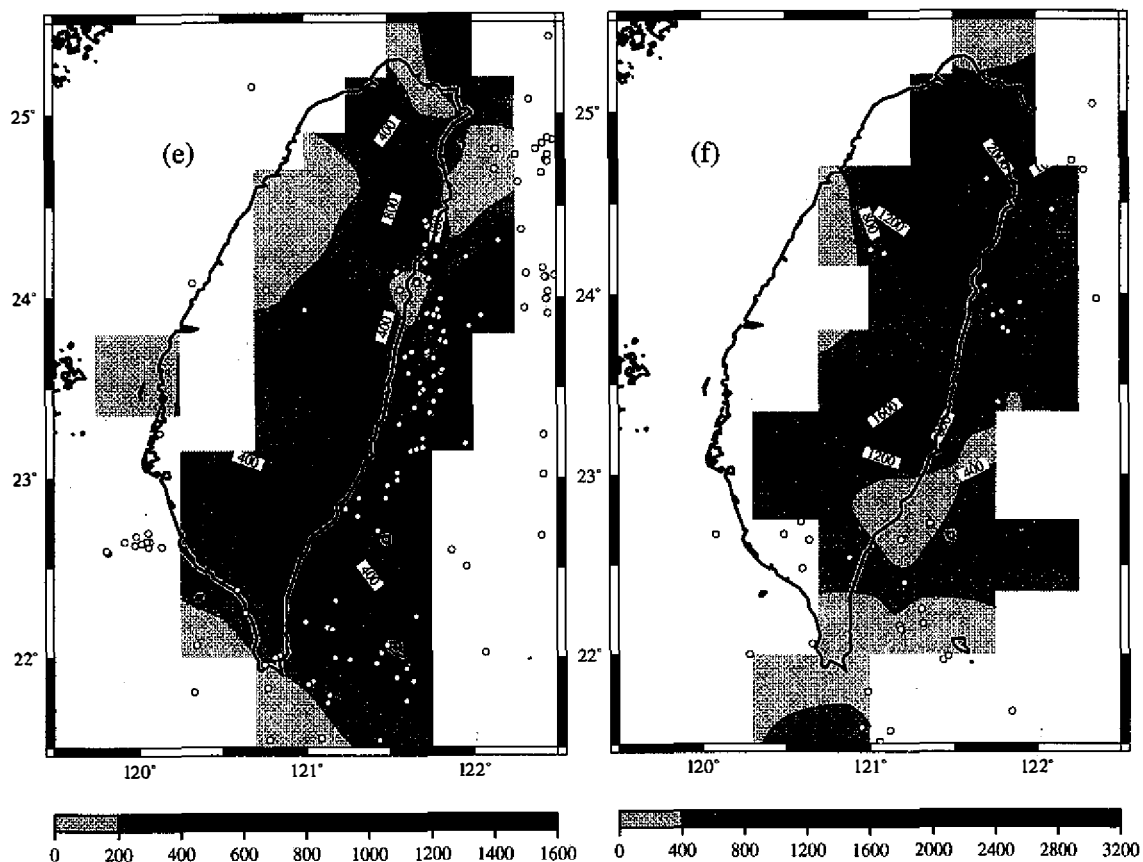
In the depth range of 35 to 50 km (layer 6), most of the Q_s values are greater than those in the upper layers, with a range of 140 to 2631 (Figure 6f), and an average of about 500. About 43% of the blocks have Q_s values less than 600. Only 10% of the blocks have values less than 300. The standard error is slightly less than 5. Three local Q_s highs can be found in this layer. They are located near Hsinchu, Taitung and the off the Ilan Plain. The local lows off the Ilan Plain in layer 4 and 5 are replaced by Q_s local high. About 75% of the earthquakes occurred in Q_s zones lower than 800 (Figure 7f).

In the depth range of 50 to 75 km (layer 7), the Q_s values range between 135 and 2066 (Figure 6g). The Q_s values on the land are slightly greater than 400. The average of this layer is about 550. About 60% of the blocks have Q_s values less than 400. The standard error is slightly less than 2. One local high almost totally covers the Puli Basin. The local Q_s high off the Ilan Plain still exist. 60% of earthquakes occurred in Q_s zones lower than 800 (Figure 7g).

In depths greater than 75 (layers 8 and 9), the lateral changes in the Q_s values are not

Layer 5 (25 - 35 km)

Layer 6 (35 - 50 km)



(Continued)

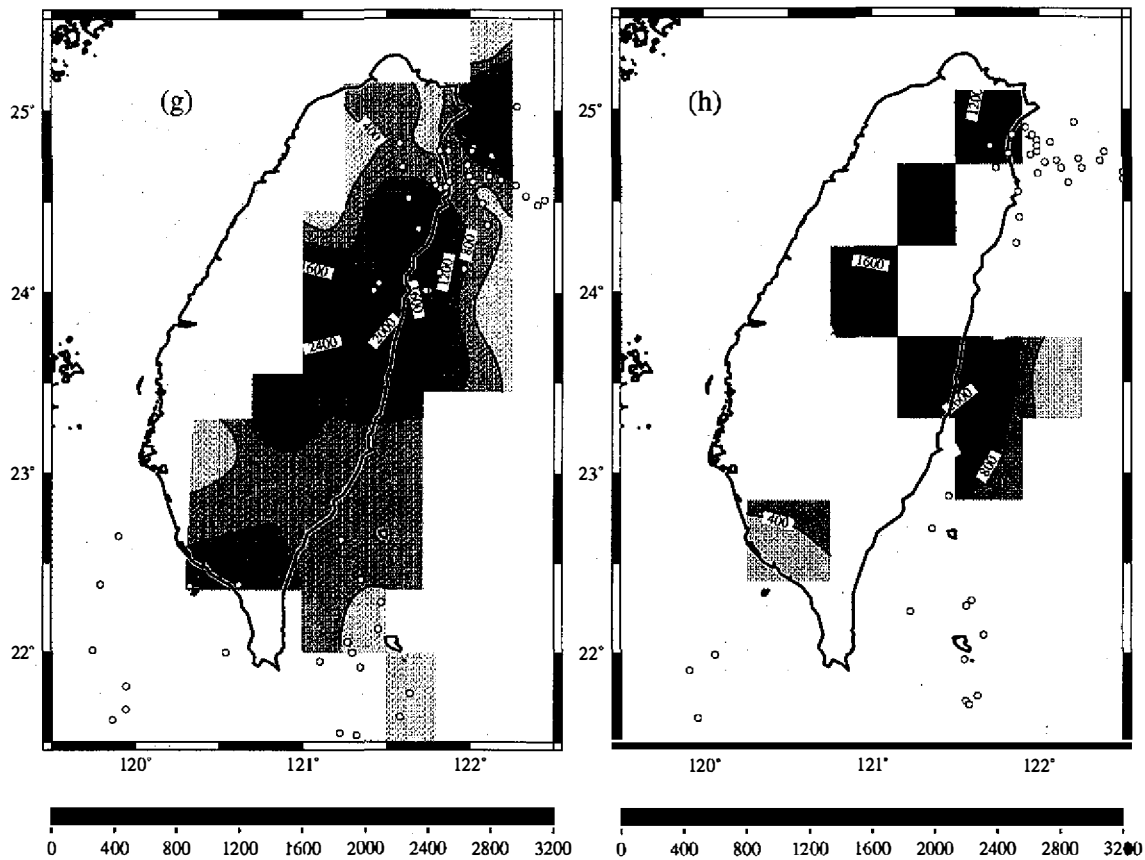
considered because only a few regions of the half space were passed by rays.

In general, low Q_s may be caused by weakness and fracture. Obviously, in the Taiwan area higher seismicity is mostly associated with low Q_s in the upper crust. However, in the upper mantle, higher seismicity has high Q_s . This author suggests that in the low Q_s areas, the material may be in a partial melting state, which always causes flow and the elimination of the possibility of earthquakes.

The standard errors shown in Figure 6 are estimated by the regression deviation of t^* , the variation of the velocity model and the variance matrix in the inversion procedure (see Equation (12)). As presented in Equation (2), the Q values are inverted by determining the travel times and velocities. The velocity model used in this study is assumed to be "true". Actually, the accuracy of the velocity model directly affects the ray paths, the travel times or both of them. The variations in travel times are not proportional to the variations in the velocity model. Therefore, to verify and estimate the variance contributed by the velocity model is not easy. It

Layer 7 (50 - 75 km)

Layer 8 (75 - 100 km)



(Continued)

means that the uncertainty of Q_s cannot be judged directly from the variance of the velocity model.

6. CONCLUSIONS

The results of the present study indicate that Q_s structures in the Taiwan area have a good correlation with seismicity. In the upper crust (at depths between 0 to 15 km), the regions of lower Q_s are consistent with higher seismicity. However, in the lower crust and upper mantle (between 15 to 75 km), the regions of higher Q_s values are consistent with higher seismicity.

Acknowledgements The author thanks the Institute of Earth Sciences, Academia Sinica and the Central Weather Bureau for providing the earthquake data. The author would like to express his appreciation to Prof. T. L. Teng, Dr. K. L. Wen and one anonymous reviewer for making many useful suggestions to improve the manuscript. Thanks are also due to Mr. W. T.

Liang for some drawings. This work was supported by the National Science Council, ROC under Grants NSC84-2111-M-003-009.

REFERENCES

- Al-Shukri, H. J., B. J. Mitchell, and H.A.A. Ghalib, 1988: Attenuation of seismic waves in the New Madrid seismic zone. *Seism. Res. Lett.*, **59**, 133-139.
- Brune, J. N., 1970: Tectonic stress and the spectra of seismic shear waves from earthquakes. *J. Geophys. Res.*, **75**, 4997-5009.
- Chen, K. J., 1993: Distribution of Q_p in the Taiwan area and its characteristics, Ph.D. dissertation, National Taiwan University (in Chinese).
- Chen, K. J., Y. H. Yeh, and C. T. Shyu, 1996: Q_p structure in the Taiwan area and its correlation to seismicity. *TAO*, **7**, 409-429.
- Der, Z. A., and T. W. McElfresh, 1976: Short period P wave attenuation along various paths in North America as determined from P wave spectra of the Salmon nuclear explosion. *Bull. Seism. Soc. Am.*, **66**, 1609-1622.
- Der, Z. A., and T. W. McElfresh, 1977: The relationship between anelastic attenuation and regional amplitude anomalies of short-period P-waves in North America. *Bull. Seism. Soc. Am.*, **67**, 1303-1317.
- Der, Z. A., T. W. McElfresh, and A. O'Donnell, 1982: An investigation of the regional variation and frequency dependence of anelastic attenuation in the mantle under the United States in the 0.5-4 Hz band. *Geophys. J. R. Astr. Soc.*, **69**, 67-100.
- Der, Z. A., T. W. McElfresh, R. Wagner, and J. Burnetti, 1985: Spectral characteristics of P wave from nuclear explosions and yield estimation. *Bull. Seism. Soc. Am.*, **75**, 379-390.
- Hanks, T. C., 1979: b-value and seismic source models: implications for tectonic stress variations along active crustal fault zones and the estimation of high-frequency strong ground motion. *J. Geophys. Res.*, **84**, 2235-2242.
- Ho, C. S., 1986: An introduction to the geology of Taiwan: Explanatory text of the geological map of Taiwan: Cent. Geol. Surv., Ministry of Econ. Affairs, R.O.C., 164pp.
- Hough, S. E., J. G. Anderson, J. Brune, F. Vernon, III, J. Berger, J. Fletcher, L. Harr, T. Hanks, and L. Baker, 1988: Attenuation near Anza, California. *Bull. Seism. Soc. Am.*, **78**, 672-691.
- Hough, S. E., and J. G., Anderson, 1988: High-frequency spectra observed at Anza, California: implications for Q structure. *Bull. Seism. Soc. Am.*, **78**, 692-707.
- Kanamori, H., 1967a: Spectrum of short-period core phases in relation to the attenuation in the mantle. *J. Geophys. Res.*, **72**, 2181-2186.
- Kanamori, H., 1967b: Spectrum of P and PcP in relation to the mantle-core boundary and attenuation in the mantle. *J. Geophys. Res.*, **72**, 559-571.
- Kanamori, H., and D. L. Anderson, 1977: Importance of dispersion in surface wave and free oscillation problems: *Review. Rev. Geophys. Space Phys.*, **15**, 105-112.

- Knopoff, L., 1964: *Q. Rev. Geophys.*, **2**, 625-660.
- Lee, W. B., and S. C. Solomon, 1978: Simultaneous inversion of surface wave phase velocity and attenuation: Love waves in Western North America. *J. Geophys. Res.*, **83**, 3389-3400.
- Lundquist, G. M. and V. C. Cormier, 1980: Constraints on the absorption model of Q . *J. Geophys. Res.*, **85**, 5244-5266.
- Mitchell, B. J., 1980: Frequency dependence of shear wave internal friction in the continental crust of eastern North America. *J. Geophys. Res.*, **85**, 5212-5218.
- Mitchell, B. J., 1981: Regional variance and frequency dependence of Q_p in the crust of the United States. *Bull. Seism. Soc. Am.*, **71**, 1531-1538.
- Modiano, T. and D. Hatzfeld, 1982: Experimental study of the spectral content for shallow earthquakes. *Bull. Seism. Soc. Am.*, **72**, 1739-1758.
- Roecker, S. W., Y. H. Yeh, and Y. B. Tsai, 1987: Three-dimensional P and S wave velocity structures beneath Taiwan: Deep structure beneath an arc-continental collision. *J. Geophys. Res.*, **92**, 10547-10570.
- Solomon, S. C., 1972: Seismic wave attenuation and partial melting in the upper mantle of North America. *J. Geophys. Res.*, **77**, 1483-1502.
- Solomon, S. C., 1973: Shear wave attenuation and melting beneath the mid-Atlantic ridge. *J. Geophys. Res.*, **78**, 6044-6059.
- Teng, T. L., 1968: An attenuation of body waves and the Q structure of the mantle. *J. Geophys. Res.*, **73**, 2195-2208.
- Thurber, C. H. and W. L. Ellsworth, 1980: Rapid solution of ray tracing problems in heterogeneous media. *Bull. Seism. Soc. Am.*, **70**, 1137-1148.